Journal of Power Sources 183 (2008) 485–490

Contents lists available at ScienceDirect

Journal of Power Sources

journal homepage: www.elsevier.com/locate/jpowsour

Electrochemical and microstructural analysis of nickel–yttria-stabilized zirconia electrode operated in phosphorus-containing syngas

Mingjia Zhi[a], Xinqi Chen[b], Harry Finklea[c], Ismail Celik[a], Nianqiang Q. Wu[a,*]

[a] Department of Mechanical and Aerospace Engineering, West Virginia University, Morgantown, WV 26506-6106, USA
[b] NUANCE Center, Northwestern University, Evanston, IL 60208, USA
[c] C. Eugene Bennett Department of Chemistry, West Virginia University, Morgantown, WV 26506, USA

ARTICLE INFO

Article history:
Received 6 March 2008
Received in revised form 21 May 2008
Accepted 21 May 2008
Available online 28 May 2008

Keywords:
Solid oxide fuel cell
Anode
Degradation
Syngas
Impurity

ABSTRACT

Trace impurities in coal-derived syngas pose a threat on the performance and durability of solid oxide fuel cells (SOFCs) operated in syngas. A Ni–YSZ/YSZ/Ni–YSZ (YSZ stands for yttria-stabilized zirconia) half-cell is constructed in order to evaluate the effects of a phosphorus impurity on the performance of the Ni–YSZ cermet anode in the simulated coal-derived syngas containing 30.6% H_2, 30% CO, 11.8% CO_2, 27.6% H_2O and 20 ppm PH_3. Electrochemical impedance analysis shows that both the charge transfer resistance and the diffusion resistance increase with time during exposure to the P-containing syngas. The diffusion resistance increases faster than the charge transfer resistance. X-ray diffraction (XRD) and X-ray photoelectron spectroscopy (XPS) studies show that phosphorus is incorporated into the Ni–YSZ electrode, leading to the formation of secondary phases of nickel phosphate and zirconium phosphate. The incorporation of phosphorus into the anode is accelerated by an applied electric field.

1. Introduction

A solid oxide fuel cell (SOFC) is an electrochemical device that directly converts chemical energy of fuels to electrical energy. SOFCs have greater fuel flexibility than other types of fuel cells, which allows SOFCs to operate, in principle, with any combustible fuel [1–3]. So far, H_2 [4,5], natural gas [6], biogas [7] as well as coal-derived syngas have been used in SOFCs [8–10]. The use of syngas derived from coal or biomass has received much attention in recent years [11–13]. Direct utilization of coal-derived syngas (CSG) as the fuel for SOFCs increases the energy efficiency and reduces the operation cost of power generation, enables the co-production of other marketable commodities such as hydrogen, and provides flexibility for carbon dioxide sequestration [14]. However, coal-derived syngas generally contains various trace impurities such as phosphorus, arsenic, mercury, selenium, vanadium and zinc [15–17]. SOFC anodes that are operated in such 'dirty' CSG gases are subject to degradation due to the attack of the trace impurities. Among all the impurities in the coal syngas, phosphorus compounds could cause severe performance degradation of SOFC anodes. Krishnan et al. have found that 10 ppm HPO_2 in the fuel causes the reduction of the SOFC power output at 750 and 800 °C [18]. Trembly et al. also have concluded that the P-containing vapor reacts with the Ni anode material to form Ni_5P_2 [19]. However, at a high partial pressure of oxygen in the coal syngas (H_2O and CO_2), it is possible that PH_3 is oxidized to the thermodynamically favored P_2O_5 [19]. Based on Krishnan's calculation, PH_3(g) would be hydrolyzed to form HPO_2 vapor at atmosphere pressure at 700–900 °C [18]. However, the microstructure evolution of the Ni–YSZ electrode in the P-containing syngas remains unclear.

In the present work, the electrochemical behavior of the Ni–YSZ anode in 'dirty' syngas is reported. Also, the degradation mechanism of the Ni–YSZ anode in the PH_3-containing syngas is discussed. Understanding the fundamental degradation mechanism of the SOFC anode operated in impurity-containing syngas is important not only for ensuring the longer life time of SOFC systems but also for developing new anode materials that resist the attack of impurities.

2. Experimental methods

A symmetrical Ni–YSZ/YSZ/Ni–YSZ half cell was constructed in this study, where YSZ stands for 8 mol% yttria-stabilized zirconia. Fig. 1 shows the configuration of the half-cell. A 150 μm thick YSZ disc was used as the electrolyte. A 50 μm thick NiO/YSZ cermet (50/50) was screen-printed on the two sides of the YSZ disc as the working and the counter electrodes (WKG and CTR). A Pt ring (approximate 1 mm wide) was painted near the edge of the electrolyte disc on the WKG side as the reference electrode (REF). The separation between the REF and the WKG was about 2 mm to avoid

* Corresponding author. Tel.: +1 304 293 3111x2335; fax: +1 304 293 6689.
E-mail address: nick.wu@mail.wvu.edu (N.Q. Wu).

0378-7753/$ – see front matter © 2008 Elsevier B.V. All rights reserved.
doi:10.1016/j.jpowsour.2008.05.055

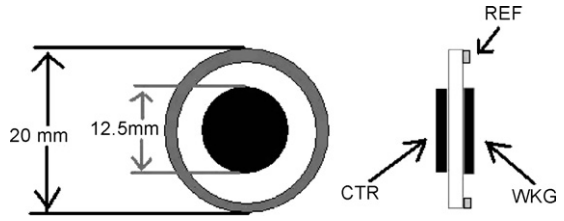

Fig. 1. Configuration of the half-cell.

the adverse effect of the alignment of the reference electrode [20]. Ni mesh strips with nickel paste in contact with each Ni–YSZ electrode were used as the current collectors.

The half-cell was placed at the center of a quartz tube inside a tube furnace. A thermocouple was placed adjacent to the half-cell to monitor the temperature. The electrode was heated to 650 °C at 1 °C min^{-1} in N_2 prior to testing. H_2 was introduced and the cell temperature was raised to 900 °C to reduce NiO to Ni. The quartz tube was fed with three types of fuel gases: (i) H_2 + 3% H_2O, (ii) simulated clean coal syngas (30.6% H_2, 30% CO, 11.8% CO_2, and 27.6% H_2O), and (iii) simulated coal syngas containing 20 ppm PH_3. The P impurity was introduced to the quartz tube with a PH_3/N_2 gas mixture. The total flow rate was controlled in the range from 150 to 200 sccm (standard cubic centimeter per minute) by the mass flow controllers. A humidity bottle was employed to achieve the desired water vapor partial pressure. A direct current (DC) load was applied between the working electrode and the counter electrode. Two leads were connected to the working electrode and the reference electrode to obtain electrochemical impedance spectroscopy (EIS). The impedance spectra were measured with a Solartron SI 1260 impedance/grain-phase analyzer at AC amplitude of 10 mV at frequencies ranging from 300 kHz to 0.1 Hz. The impedance data were fitted by the commercial Zview© software to obtain the parameters in the simulated equivalent circuit. In addition, a plot of current density as a function of time was obtained when +0.7 V DC bias was applied between the working electrode and the counter electrode.

The morphology of the Ni–YSZ anode was examined with a Hitachi S-4700 scanning electron microscope (SEM). The crystal structure of the anode was determined with a Panalytical X-ray diffractometer (XRD) equipped with a thin film stage. The chemical status and chemical composition of the anode was characterized with an Omicron ESCA PROBE X-ray photoelectron spectroscopy (XPS). XPS was performed with a monochromatic Al Kα radiation (1486.6 eV) with an operating power of 300 W.

3. Results and discussions

3.1. Electrochemical measurement

A half-cell was exposed to different fuel gases at 900 °C. A DC bias of 0.7 V was applied between the working electrode and the counter electrode to drive the current through the cell. The WKG electrode bias was positive to drive the oxidation of hydrogen to water. The CTR electrode was simultaneously reducing water vapor to hydrogen. The cell was initially exposed to the wet H_2 gas (97% H_2 + 3% H_2O) for 4 h. The feed gas was then switched to the clean syngas for 12 h, followed by the dirty syngas containing 20 ppm PH_3 for an additional 12 h. It can be seen from Fig. 2 that the current density of 0.75 A cm^{-2} remained constant during exposure to the wet H_2 gas. When the fuel gas was switched to the simulated clean syngas, the current density dropped immediately. The lower current density is attributed to the lower rates of mass of transfer of CO relative to H_2. While exposed to the clean syngas condition, the current density was very stable. When 20 ppm PH_3 was introduced into the syngas,

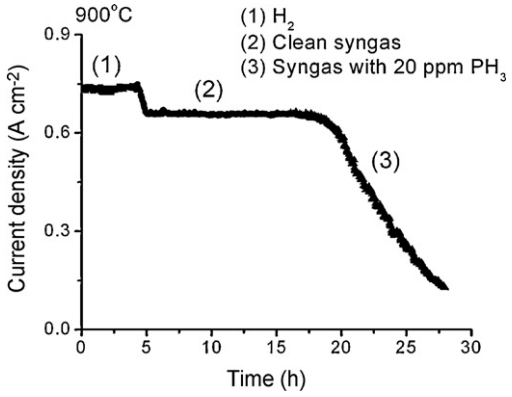

Fig. 2. Effect of the fuel gas on the DC current (driven by the DC bias of 0.7 V).

the current density decreased steadily with time, suggesting that the cell was undergoing degradation and that the total resistance (ohmic, polarization and mass transfer) of the cell was increasing.

To probe the underlying degradation mechanism of the half-cell in the PH_3-containing syngas, two sets of electrochemical impedance data were obtained. One set was acquired at the open circuit (no DC current between the working electrode and the counter electrode). The other set was acquired at the loading potential of +0.7 V (WKG electrode vs. CTR electrode). The impedance data were collected every 4 h. Two arcs were observed in the Nyquist plots of impedance (Fig. 3). The intercept of the high frequency arc yielded the ohmic series resistance of the cell. It exhibited a low

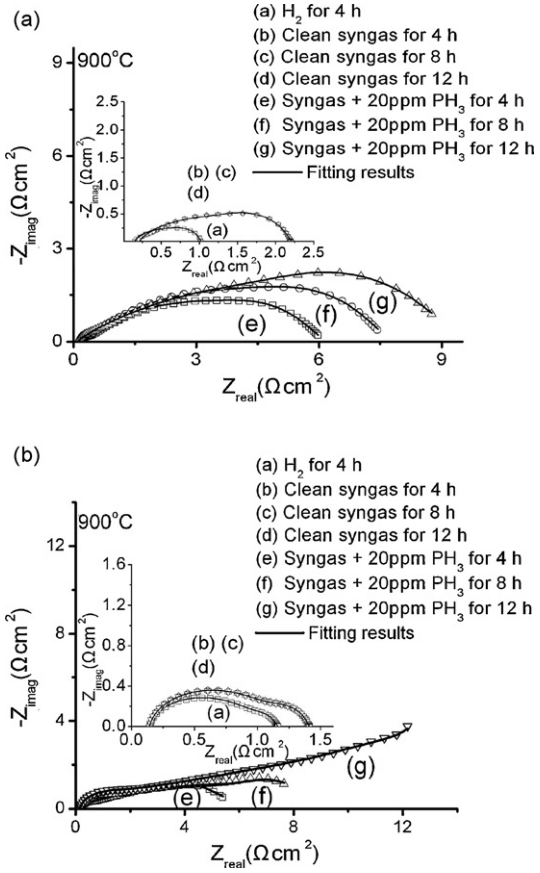

Fig. 3. Nyquist plot of impedance obtained from the half-cell at 900 °C: (a) under the open circuit condition and (b) at +0.7 V potential applied between the working electrode and the counter electrode.

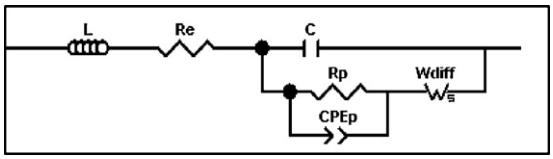

Fig. 4. Equivalent circuit model of the impedance spectra.

value ($0.2\,\Omega\,cm^2$) and was invariant within experimental uncertainty during the successive gas exposures. The impedance plot did not change after the half-cell was exposed to the clean syngas for 12 h, which implies that the cells were not subject to any noticeable degradation during exposure to the clean syngas. However, after 20 ppm PH_3 was introduced into the reactant gas, the total polarization resistance of the electrode increased with the exposure time.

In Fig. 3, the arc at the high frequency regime with the characteristic frequency of $\sim 10^4$ Hz is attributed to the impedance of the charge transfer processes occurring at the electrolyte/electrode interface and at the Ni/YSZ interface, because the characteristic frequency of such processes usually is larger than 10^4 Hz [21,22]. The arc at the low frequency regime (characteristic frequency ca. 10^2 Hz) is attributed to the bulk capacitance and the chemical processes including adsorption, surface migration, bulk migration, and other mechanistic steps. An equivalent circuit model is proposed (Fig. 4) to interpret the experimental impedance data. In this model, L is defined as the inductance associated with the long leads from the impedance system to the half-cell. C is the bulk capacitance. R_e represents the resistance of the electrolyte and the contact resistance of the whole circuit. R_p is the charge transfer resistance that controls the Faradaic current. CPE_p is a double-layer constant phase element. The impedance of CPE can be expressed by $Z_{CPE} = 1/Y(j\omega)^n$ where Y is the pseudo-capacitance, ω is radial frequency ($\omega = 2\pi f$) and n is the exponent constant. W_{diff} is the Warburg diffusion element that reflects the gas diffusion to the electrode. The Warburg impedance can be expressed by $Z_W = R_w \tanh(jY\omega)^{0.5}/(jY\omega)^{0.5}$. R_w is derived from the Warburg diffusion element and represents the diffusion resistance.

The low frequency arc was pulled down toward the Z_{real}-axis when either the H_2 concentration or the DC bias increased (Fig. 3). As the DC bias increased from 0 to +0.7 V, the charge transfer resistance R_p decreased while the diffusion resistance remained almost constant (data not shown here). Obviously, this trend suggests that R_p is governed by an electrochemical reaction, because only the impedance corresponding to charge transfer of an electrochemical reaction can be reduced by an applied bias [23] as indicated by Butler–Volmer equation [24]. It is not surprising that the gas diffusion remains constant, as indicated by the constant value of the Warburg element, because diffusion is dependent on the concentration gradient, as determined by the partial pressure of the reactants H_2 or H_2O in the gas phase and in the reaction zone next to the electrolyte.

The values of the circuit elements at the different conditions were calculated as listed in Table 1. The ohmic series resistance was 0.18–0.24 $\Omega\,cm^2$. The values of R_p and R_w under different conditions are graphically compared in Fig. 5. The R_p and R_w values for two sets of impedance data are normalized with respect to the initial values in the wet hydrogen gas so that the relative increase in these parameters can be compared. Both R_p and R_w values in the clean syngas are larger than the corresponding values in the wet H_2 gas, which is consistent with the drop in DC current upon changing from wet hydrogen to the clean syngas. Both R_p and R_w remain constant during exposure either to the clean syngas or to the wet H_2 gas. However, both the charge transfer resistance

Table 1
Parameters of the equivalent circuit at the different conditions at 900 °C

	R_p ($\Omega\,cm^2$)	R_w ($\Omega\,cm^2$)	χ^2
Open circuit			
H_2	0.61	0.33	1.8E−5
Clean syngas	0.87	0.70	1.7E−5
Syngas + 20 ppm PH_3, 4 h	5.01	0.99	2.8E−5
Syngas + 20 ppm PH_3, 8 h	6.12	1.51	3.3E−5
Syngas + 20 ppm PH_3, 12 h	7.11	2.52	2.9E−5
Loaded			
H_2	0.93	0.12	5.8E−6
Clean syngas	1.02	0.26	2.4E−6
Syngas + 20 ppm PH_3, 4 h	5.23	1.09	8.5E−6
Syngas + 20 ppm PH_3, 8 h	8.36	2.38	4.2E−6
Syngas + 20 ppm PH_3, 12 h	15.74	6.90	3.2E−6

Note: χ^2 reflects the deviation of the experimental data and the fitting data.

(R_p) and the diffusion resistance (R_w) increase with time during exposure to the PH_3-containing syngas. This increase suggests that the incorporation of phosphorus impurity into the electrode not only impedes the charge transfer but also blocks the channels of gas diffusion. The normalized diffusion resistance increases faster than the normalized charge transfer resistance. The impedance plot after 12 h of exposure to the P-containing syngas at a loading of +0.7 V shows a linear tail at low frequencies (Fig. 3(b)), implying that the impedance is dominated by the diffusion of the reactant gases. This observation suggests that the porous microstructure of the electrode was destroyed. Furthermore, both the charge transfer resistance and the diffusion resistance under the loading potential are larger than those resistances at the open circuit. In other words, the application of an electric field appears to accelerate the degradation of the electrode in the 'dirty' syngas. The evidence presented below suggests that the degradation occurs at the anode.

3.2. Analysis of chemical composition and microstructure of anode

In order to elucidate the reason for the change in both the charge transfer resistance and the diffusion resistance in the 'dirty' syngas, the microstructural evolution of the Ni–YSZ working electrode was examined after exposure to the PH_3-containing syngas. The CTR electrode was not examined, because attention was focused on the electrode at which the fuel gas is oxidized in the SOFC. Fig. 6 shows the SEM images of the working electrode of the half-cell. The Ni–YSZ electrode shows a well-defined matrix structure with the presence of many pores after exposure to the clean

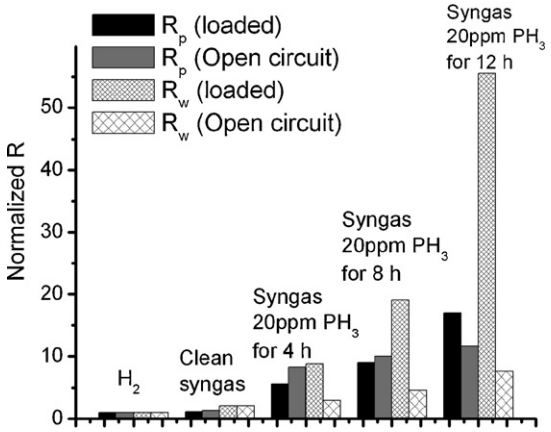

Fig. 5. Charge transfer resistance (R_p) and diffusion resistance (R_w) derived from the impedance spectra obtained at 900 °C.

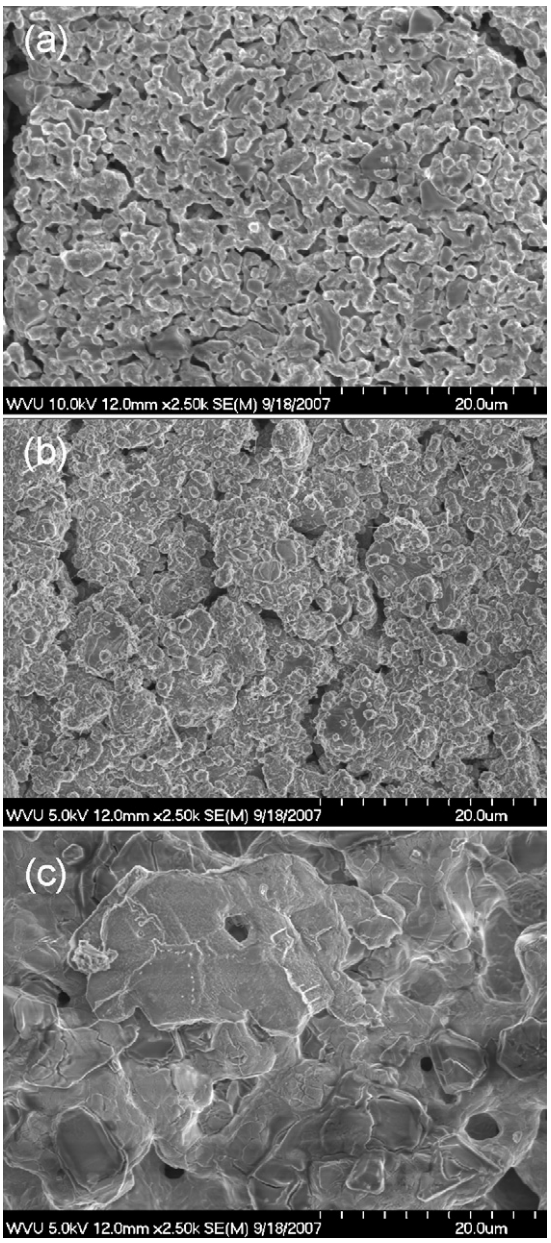

Fig. 6. SEM images of the Ni–YSZ working electrode surface: (a) the electrode after exposure to the clean syngas (clean cell), (b) the electrode after exposure to the PH_3-containing syngas at the open circuit and (c) the electrode after exposure to the PH_3-containing syngas at the applied DC bias of 0.7 V.

syngas (Fig. 6(a)). After exposure to the 'dirty' syngas, the particles in the electrode were coarsened and the porosity was significantly reduced (Fig. 6(b)). At the DC bias of 0.7 V, the structure became much worse (Fig. 6(c)). The round-shaped particles disappeared on the electrode surface while the flat flake-like particles appeared. The porosity was reduced remarkably, leading to severe blockage of the gas channels. Therefore, it is understandable that the impedance plot shows a Warburg tail after 12 h of exposure to the 'dirty' syngas at a loading of 0.7 V (Fig. 3(b)).

Fig. 7 reveals the XRD patterns obtained from the Ni–YSZ working electrode. Metallic Ni and YSZ were the major phases observed in the electrode after exposure to the clean syngas (Fig. 7(a)). A trace amount of NiO was found in this sample. The formation of NiO may be due to the exposure of the electrode to moisture during cooling. After exposure to the PH_3-containing syngas at the open

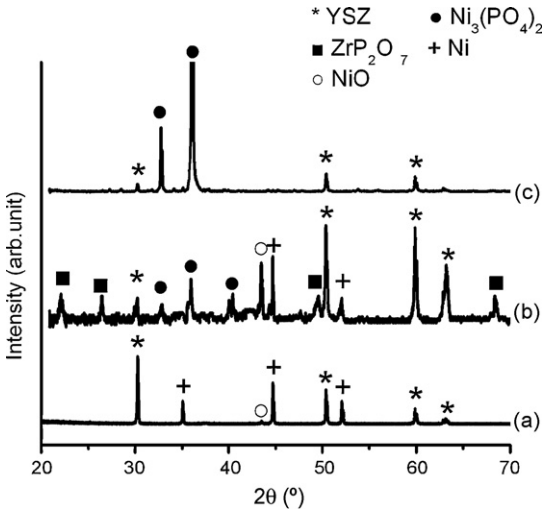

Fig. 7. XRD patterns of the Ni–YSZ working electrode: (a) the electrode after exposure to the clean syngas (clean cell), (b) the electrode after exposure to the PH_3-containing syngas at the open circuit (open circuit cell) and (c) the electrode after exposure to the PH_3-containing syngas at the applied DC bias of 0.7 V (loaded cell).

circuit, $Ni_3(PO_4)_2$ and ZrP_2O_7 were found in the electrode besides YSZ, Ni and NiO (Fig. 7(b)). For the loaded cell (Fig. 7(c)), metallic Ni completely disappeared and the amount of YSZ was reduced considerably. In this case, $Ni_3(PO_4)_2$ was the dominant phase, although a small amount of YSZ was present.

In the present work, such a low concentration of PH_3 is enough to convert a large amount of Ni to $Ni_3(PO_4)_2$, because the P-containing compound can be concentrated in the adsorbate on the solid surface. Similar phenomena have been reported in previous studies [16]. For example, 1 ppm AsH_3 in the syngas was able to convert Ni to NiAs in the SOFC anode [16]. In addition, YSZ coatings used in land-based industrial engines and sea engines are usually operated with low-quality fuels containing sulfur and vanadium in the range of <100 ppm [25]. After combustion, the V_2O_5 content in the ash deposit on the coating surface can be concentrated to a much higher level, leading to severe corrosion of YSZ due to the attack by the concentrated V impurity in the adsorbate on the YSZ surface [26].

Although the P impurity is introduced to the fuel gas with the form of PH_3, it may be converted to other forms under the equilibrium condition at the testing temperature. To account for the formation of phosphate phases, the following reaction may be considered under the testing conditions:

$$PH_3(g) + 4H_2O(g) = H_3PO_4(g) + 4H_2(g) \quad (1)$$

The Gibbs free energy change for the above reaction is $-407.8\ kJ\ mol^{-1}$ based on the calculation with the thermodynamic data provided by the National Institute of Standard and Technology (NIST) database [27]. The conversion of PH_3 to H_3PO_4 in the gas phase is thermodynamically favored under the testing condition. The phosphoric acid formed can attack the nickel electrode and YSZ electrolyte to form corresponding phosphate species. Therefore, it is not surprising that nickel phosphate is formed rather than nickel phosphide.

XPS was used to examine the outer surface layer of the working electrode, where the electrode surface is directly exposed to the PH_3-containing syngas. Survey scans were performed to identify the elemental composition of the electrode surface. Detailed scans of the specific core levels of individual elements were employed to examine the chemical structure of the electrode surface. Fig. 8

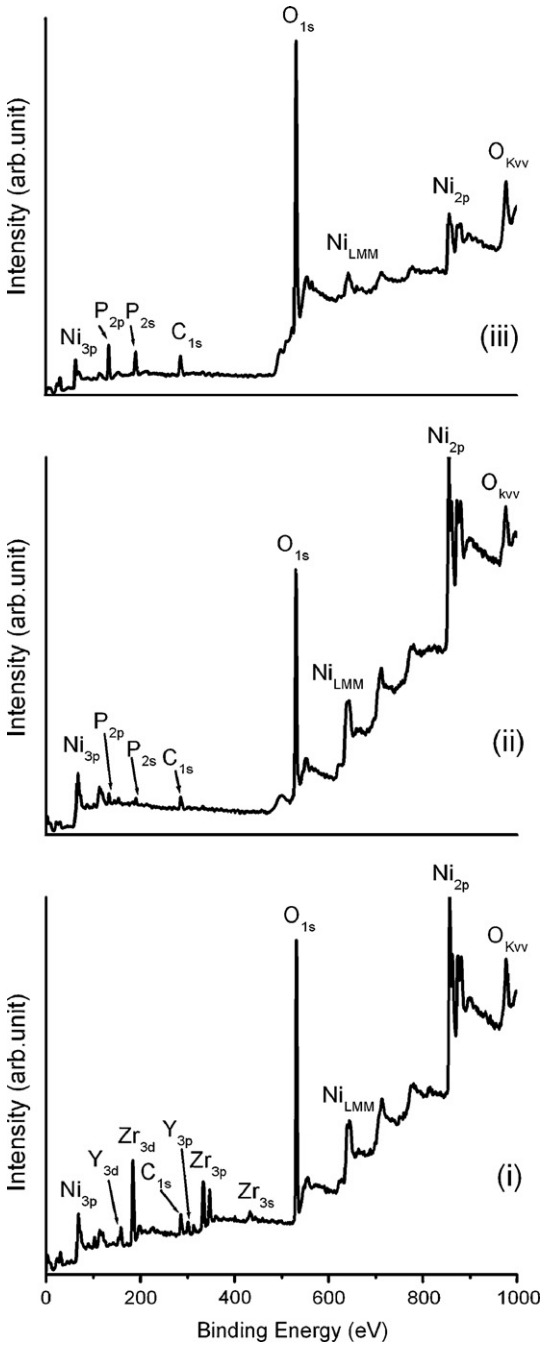

Fig. 8. Survey scan of the XPS spectra obtained from the Ni–YSZ working electrode under different experimental conditions: (i) the electrode after exposure to the clean syngas (clean cell), (ii) the electrode after exposure to the PH_3-containing syngas at the open circuit (open circuit cell), and (iii) the electrode after exposure to the PH_3-containing syngas at the applied DC bias of 0.7 V (loaded cell).

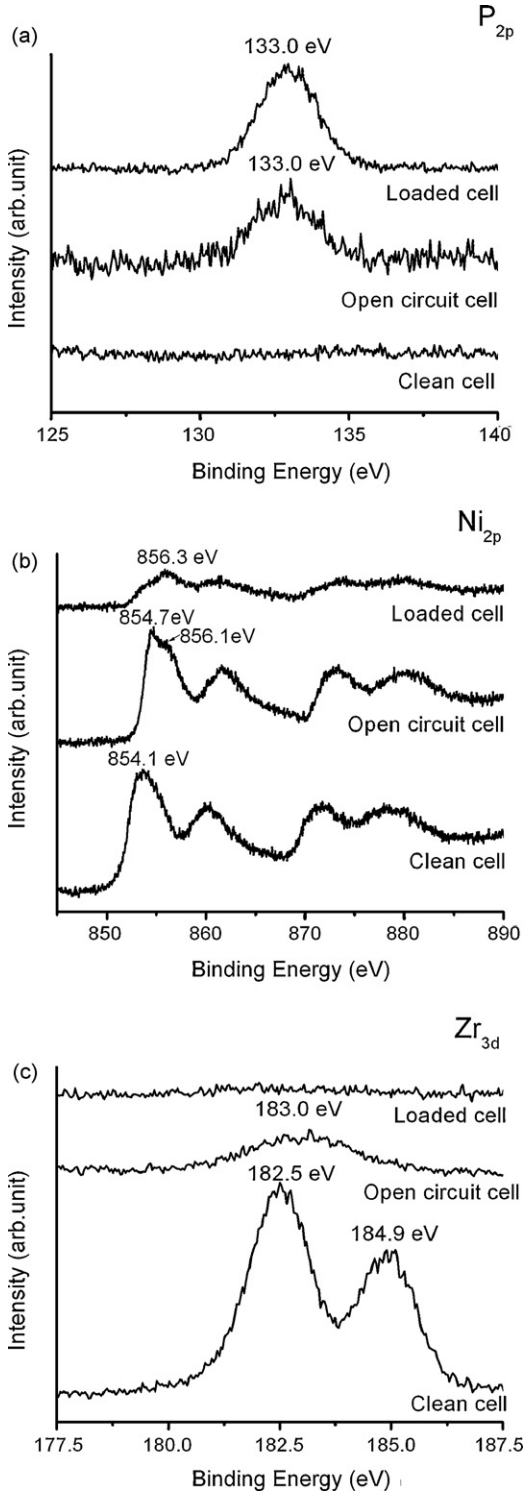

Fig. 9. (a) XPS spectrum of the P 2p core level, (b) XPS spectrum of the Ni 2p core level and (c) XPS spectrum of the Zr 3d core level.

shows the survey scan of the Ni–YSZ working electrodes. Phosphorus was not detected in the XPS spectrum of the electrode after exposure to the clean syngas (clean cell). In contrast, the P 2p peaks appeared in the spectrum of the electrode after exposure to the PH_3-containing syngas at the open circuit, and the intensity of the Zr 3d peaks decreased significantly. After exposure to the PH_3-containing syngas at an applied DC bias of 0.7 V, only the peaks associated with P, Ni and O were found in the XPS spectrum. The Zr peaks completely disappeared. One mechanism accounting for this observation requires nickel to diffuse outward to the electrode surface under the applied electric field. This process accelerates the reaction of Ni with P impurity, and thus buries the YSZ underneath the $Ni_3(PO_4)_2$ layer. The underlying mechanism of the accelerated incorporation of P into the electrode by an applied DC bias needs to be further studied in detail in the future. One of the possible causes is electromigration, a common diffusion phenomenon [28,29]. Electromigration is the mass transport induced by the gradual movement of the ions in a conductor due to the

momentum transfer between conducting electrons and diffusing atoms. Two driving forces are responsible for the migration of the ionized atoms [28]. One is the direct force that exerts direct action of the external field on the charge of the migrating ion. Another is the "electron wind" force from the exchange of momentum with other charge carriers. Electromigration has drawn intense attention in metal/semiconductor systems [30]. Recently, electromigration was suggested to be responsible for the re-distribution of elements at the Ni–YSZ interface in a SOFC [31].

Fig. 9(a)–(c) reveals the detailed scans of the P 2p, Ni 2p, and Zr 3d core levels, respectively. The P 2p peak at 133 eV is assigned to phosphates [32]. The Ni $2p_{3/2}$ peak at 854.1–854.7 eV corresponds to nickel oxide [33]. The Ni $2p_{3/2}$ peak at 856.3 eV is assigned to nickel phosphate [34]. The Zr 3d doublet centered at 182.5 and 184.9 eV is in agreement with the reported values for YSZ [35]. The Zr $3d_{5/2}$ peak at 183.0 eV is attributed to zirconium phosphate [36]. In the XPS spectra of the electrode after exposure to the clean syngas (clean cell), no P peak was found while the intensity of the Zr 3d peak was very strong. After exposure to the 'dirty' syngas, the P peak became clearly visible while the height of the Zr 3d peak was reduced considerably. At a loading of 0.7 V, Zr was not detected.

XPS and XRD measurements have clearly demonstrated that the secondary phases are formed due to the incorporation of P into the electrode. The conversion of metallic Ni to nickel phosphate causes the electrode to lose the electrocatalytic activity toward oxidation of the fuel gas. The transformation of YSZ to ZrP_2O_7 inhibits the ability of the electrode to transport oxygen ions in the electrode. Therefore, the charge transfer resistance increases with time during exposure to the PH_3-containing syngas.

4. Conclusions

The presence of 20 ppm PH_3 in coal syngas causes a poisoning effect on the working electrode of the Ni–YSZ/YSZ/Ni–YSZ half cell. An equivalent circuit model is proposed to interpret the impedance data obtained. Both the charge-transfer resistance and the diffusion resistance of the Ni–YSZ electrode dramatically increase with time during exposure to the PH_3-containing syngas. The diffusion resistance increases proportionally faster than the charge transfer resistance. The electric field appears to accelerate the degradation of the Ni–YSZ electrode. During exposure to the dirty syngas, the phosphorus species derived from phosphine react with Ni and Zr to form phosphates in the Ni–YSZ electrode, which suppresses the electrocatalytic activity of the electrode. The incorporation of phosphorus into the electrode and the subsequent formation of the secondary phases cause the blockage of the gas diffusion channels and the loss of the charge transport pathways.

Acknowledgments

This work is financially sponsored by the US Department of Energy (DOE) EPSCoR Program (grant number: DE-FG02-06ER46299). It is jointly sponsored by US DOE Office of Basic Energy Sciences, National Energy Technology Laboratory (NETL), the WV State EPSCoR Office and West Virginia University. Dr. R. Bajura is the Administrative Manager and Dr. I. Celik is the Technical Manager. Dr. Wu acknowledges the fruitful discussions with Dr. Christopher Johnson at NETL, DOE.

References

[1] S. McIntosh, R.J. Gorte, Chem. Rev. 104 (2004) 4845–4865.
[2] S.C. Singhal, Solid State Ionics 135 (2000) 305–313.
[3] S.P. Jiang, S.H. Chan, J. Mater. Sci. 39 (2004) 4405–4439.
[4] H. Koide, Y. Someya, Y. Toshihiko, M. Toshio, Solid State Ionics 132 (2000) 253–260.
[5] J.H. Jiang, J.H. Ryu, S.M. Oh, Ionics 6 (2000) 86–91.
[6] J. Liu, S.A. Barnett, Solid State Ionics 158 (2003) 11–16.
[7] J. Staniforth, R.M. Ormerod, Ionics 9 (2003) 336–341.
[8] R. Suwanwarangkul, E. Croiset, E. Entchev, S. Charojrochkul, M.D. Pritzker, M.W. Fowler, P.L. Douglas, S. Chewathanakup, H. Mahaudom, J. Power Sources 161 (2006) 308–322.
[9] E.H. Pacheco, M.D. Mann, P.N. Hutton, D. Singh, K.E. Martin, Int. J. Hydrogen Energy 30 (2005) 1221–1233.
[10] J.P. Trembly, A.I. Marquez, T.R. Ohrn, D.J. Bayless, J. Power Sources 158 (2006) 263–273.
[11] O. Costa-Nunes, R.J. Gorte, J.M. Vohs, J. Power Sources 141 (2005) 241–249.
[12] A. Weber, B. Sauer, A.C. Muller, D. Herbstritt, E. Ivers-Tiffe, Solid State Ionics 152/153 (2002) 543–550.
[13] K. Sasaki, Y. Hori, R. Kikuchi, K. Eguchi, A. Ueno, H. Takeuchi, M. Aizawa, K. Tsujimoto, H. Tajiri, H. Nishikawa, Y. Uchida, J. Electrochem. Soc. 149 (2002) 227–233.
[14] T.R.S. Gemmen, J. Trembly, J. Power Sources 161 (2006) 1084–1095.
[15] Eastman Chemical Company, Project Data on Eastman Chemical Company's Chemicals-From-Coal Complex in Kingsport, TN, U.S. Dept. of Energy, 2003, 10–12.
[16] J.P. Trembly, R.S. Gemmen, D.J. Bayless, J. Power Sources 171 (2007) 818–825.
[17] S. Benson, T.A. Erickson, C.J. Zygarlicke, C. O'Keefe, K.A. Katrinak, S.E. Allan, D.J. Hassett, W.B. Hauserman, Fuel Cells Review Meeting, Morgantown, WV, August 9–10, 1995.
[18] G. Krishnan, Technical progress report 1, SRI International, Morgantown, 2006.
[19] J.P. Trembly, R.S. Gemmen, D.J. Bayless, J. Power Sources 163 (2007) 986–996.
[20] S.B. Adler, J. Electrochem. Soc. 149 (2002) E166–E172.
[21] S. Primdahl, M. Mogensen, J. Electrochem. Soc. 144 (1997) 3409–3418.
[22] S.B. Adler, Solid State Ionics 111 (1998) 125–134.
[23] N. Robertson, J.N. Michaels, J. Electrochem. Soc. 138 (1991) 1494–1499.
[24] J.R. Macdonald, W.R. Kenan, Impedance Spectroscopy, Wiley, New York, 1987, pp. 71–73.
[25] R.L. Jones, J. Electrochem. Soc. 139 (1992) 2794–2926.
[26] N.Q. Wu, Z. Chen, S.X. Mao, J. Am. Ceram. Soc. 88 (2005) 675–682.
[27] National Institute of Standard and Technology (NIST) Chemistry WebBook, NIST Standard Reference Database, Number 69, June 2005, http://webbook.nist.gov/chemistry/.
[28] P.S. Ho, Rep. Prog. Phys. 52 (1989) 301–348.
[29] H.T. Orchard, A.L. Greer, Appl. Phys. Lett. 86 (2005) 231906.
[30] H. Yasunga, A. Natori, Surf. Sci. Rep. 15 (1992) 205–208.
[31] K.V. Jenson, R. Wallenberg, I. Chorkendorff, M. Mogensen, Solid State Ionics 160 (2003) 27–37.
[32] J.F. Moulder, W.F. Stickle, P.E. Sobol, K.D. Bomben, Handbook of X-ray Photoelectron Spectroscopy, Eden Prairie, 1992, pp. 59–60.
[33] J.F. Moulder, W.F. Stickle, P.E. Sobol, K.D. Bomben, Handbook of X-ray Photoelectron Spectroscopy, Eden Prairie, 1992, pp. 85–86.
[34] S.S. Park, S.J. Choe, D.H. Park, Korean J. Chem. Eng. 20 (2003) 256–261.
[35] M.B. Pomfret, C. Stolz, B. Varughese, R.A. Walker, Anal. Chem. 77 (2005) 1791–1795.
[36] E.T. Paparazzo, E. Severini, A. Jimenez-Lopez, P. Maireles-Torres, P. Olivera-Pastor, E. Rodriguez-Castellon, A.A.G. Tomlinson, J. Mater. Chem. 2 (1992) 1175–1178.